Measurements of the Impurity Flow Velocity and Temperature in Deuterium and Hydrogen Plasmas in the Divertor Legs of the Stochastic Layer in LHD*)

Arseniy KUZMIN, Masahiro KOBAYASHI, Tomohide NAKANO[1)], Masahiro HASUO[2)], Keisuke FUJII[2)], Motoshi GOTO, Taiichi SHIKAMA[2)], Tomohiro MORISAKI and the LHD Experiment Group

National Institute for Fusion Science, 322-6 Oroshi-cho, Toki 509-5293, Japan
[1)]*National Institutes for Quantum and Radiological Science and Technology, Naka Fusion Institute, 801-1 Mukoyama, Naka-shi, Ibaraki 311-0193, Japan*
[2)]*Kyoto University, Kyotodaigaku-katsura, Nishikyo-ku, Kyoto 614-8540, Japan*

(Received 26 December 2017 / Accepted 17 April 2018)

This paper presents carbon impurity flow velocity and temperature measurements in the divertor region for a wide density range n_e = (1 - 14) $\times 10^{19}$ m^{-3}, central electron temperature T_e = 1.5 - 3.5 keV, and with total neutral beam injection power of 9 - 12 MW. The isotope effect on the transport is studied in hydrogen (H) and deuterium (D) discharges. Flow velocities for D plasma are systematically slower, by the factor of 1.4 - 2, compared to H plasma. For all selected discharges, the carbon ions flow toward the divertor in both H and D plasmas. Different velocities are obtained depending on the charge states. For C^+ and C^{2+} they are in the range of 10 - 30 km/s, and 5 - 20 km/s for C^{3+} ions. It is also found that there is no change of flow direction even in the lowest density, where the impurity transport model predicts flow toward upstream in the thermal force dominant regime. In H discharges velocities increase proportionally to the plasma density, while in D discharges this dependency is weaker. Possible mechanism to interpret these observations is discussed based on the parallel momentum balance of impurity transport.

Keywords: impurity, transport, isotope effect, carbon, deuterium, hydrogen, Echelle spectroscopy

DOI: 10.1585/pfr.13.3402058

1. Introduction

The impurity transport in the edge plasma is not yet fully understood, while its strong influence on the performance of the core plasma as well as on the tritium retention becomes more evident [1,2]. The impurity transport in the scrape-off layer (SOL) determines an influx to the core region and distribution of the impurity radiation. Understanding of the SOL impurity transport is, therefore, crucial for a good confinement and for the detachment control. The model for impurity transport in SOL, widely used in numerical simulations, still requires improvement and validation [3–5]. For this purpose, one needs systematic measurements of impurity parameters such as flow and temperature, which can be compared carefully with the numerical simulations based on the transport model.

To investigate the impurity and fuel transport in the edge plasma in greater detail, a wide wavelength range (409 - 801 nm), high resolution (~ 0.05 nm) Echelle spectrometer has been installed in LHD. Such spectroscopy makes it possible to analyze several aspects of impurity transport, such as flow velocity and temperature, local plasma parameters with collisional radiative model [6, 7], and hydrogen molecule [8]. In this paper, we present systematic measurements of impurity velocities and temperatures of different ionization states of carbon (C^+-C^{3+}) in the divertor leg region in LHD. Density dependence and isotope effects are discussed based on the current impurity transport model.

2. Experimental Set-Up

The Echelle spectrometer produces a 2D image on the CCD detector, where different diffraction orders are separated in vertical direction and shifted in horizontal direction. A raw image on the CCD detector of the spectra from typical LHD plasma is shown in Fig. 1, where the different diffraction orders are separated vertically with blank region of ten to twenty pixels, and wider separation for higher order index. The green lines indicate the borders of each diffraction order, which are selected such that areas with highest sensitivity are used, and that no overlapping of the wavelength between the different orders occurs when constructing spectra in full wavelength range. The

author's e-mail: arseniy.kuzmin@lhd.nifs.ac.jp
*) This article is based on the presentation at the 26th International Toki Conference (ITC26).

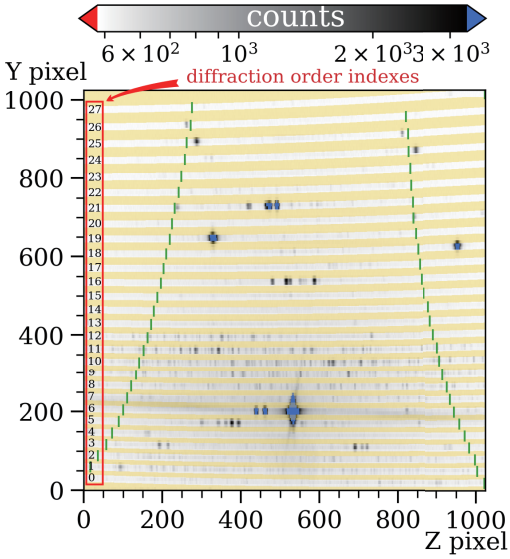

Fig. 1 Raw image of the LHD plasma emission focused on the CCD detector of the Echelle spectrometer. Gaps between orders are covered in yellow mask. Diffraction order indexes are shown at the left side. Peak intensities are in logarithmic scale.

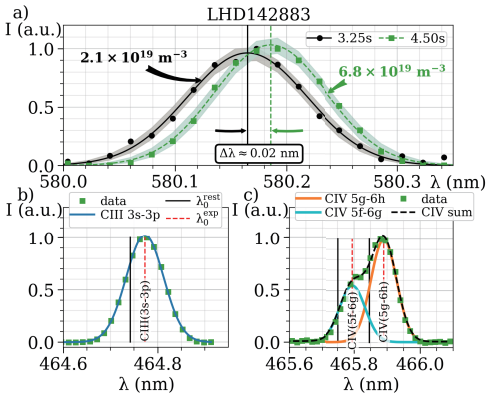

Fig. 2 a) Doppler shift of CIV line emission in LHD plasma in one discharge at t = 3.25 s, n_e = 2.1 × 10^{19} m^{-3} and t = 4.5 s, n_e = 6.8 × 10^{19} m^{-3}. b) CIII (3s-3p) line and c) CIV (5f-6g and 5g-6h) lines. I - intensity, λ - wavelength. In b) and c) λ_0^{rest} and λ_0^{exp} are center wavelengths at rest (black solid line) and in experiment (red dashed line), respectively.

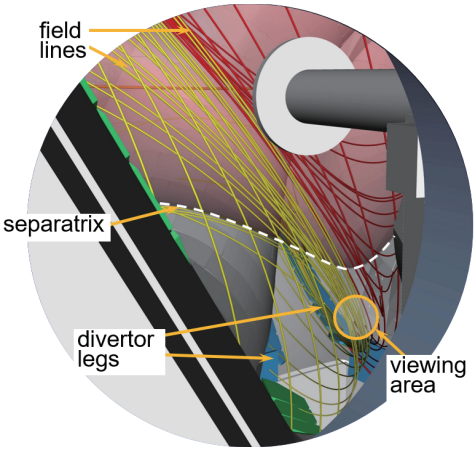

Fig. 3 Line of sight of the spectroscopy set-up. The viewing area of the spectrometer is on the divertor leg, shown by blue plates. It is almost tangential to the magnetic field lines, shown by yellow and red lines.

brightest line at $Z \sim 500$ and $Y \sim 200$ corresponds to H_α line in diffraction order #6. Fulcher-band lines around 500 to 600 nm are also noticeable in rows #10 and 11. A numerical tool was developed to convert the raw image into a spectrum. For each diffraction order, the signal is binned vertically over 8 pixels, and wavelength calibration is carefully performed using the Th-Ar, Ne and He calibration lamps with precision up to ~ 0.015 nm. This gives a systematic error in velocity of ±5 km/s. Frame rate of the data acquisition is 4 frames per second for full scan of the CCD image. Flow velocities are estimated by analyzing the Doppler shift of the spectral lines. An example of the CIV line ($1s^2 3s$-$1s^2 3p$, 580.1 nm) shift in the LHD discharge is shown in Fig. 2 a), for low and high densities, 2.1×10^{19} and 6.8×10^{19} m^{-3}, respectively. A clear shift of the spectra toward longer wavelength side is seen for high density case. In Figs. 2 b) and c) clear distinction between CIII and CIV lines, used in this research, are shown. The flow toward divertor plate is defined as negative values, i.e., flow away from the observation point (Fig. 3), $V_Z = c\frac{\lambda_0 - \lambda_1}{\lambda_0}$, c - speed of light, λ_0 - wavelength at rest, and λ_1 - wavelength of the moving ion. The shift, therefore, indicates the increase of the flow with increasing density, as discussed below. The impurity temperatures are estimated from the Doppler broadening.

$$T_Z\,[\mathrm{eV}] = 4.69 \times 10^8 \mathrm{A} \left(\frac{\sigma}{\lambda_0}\right)^2, \qquad (1)$$

where T_Z is impurity temperature and A is atomic mass of the impurity. The true width of the line at $1/e$, σ, is calculated using experimentally measured width σ_{exp} and instrumental width, σ_{inst}, as $\sigma^2 = \sigma_{exp}^2 - \sigma_{inst}^2$. The instrumental function σ_{inst} is carefully measured at room temperature, as shown in Fig. 4.

It is found that the scatter becomes larger at longer wavelength (> 600 nm), the reason for which is still under investigation. The standard deviation of the scatter increases from less than 1 % with wavelengths shorter than 600 nm to ~ 3 - 5 % with longer wavelengths.

For the present analysis, we use the spectra below 600 nm, where the scatter is substantially small.

An optical fiber array with 100 channels is situated at a window port at the outboard of LHD (4-O port), viewing the divertor region around the bottom of LHD (3.5-L port). The Echelle spectrometer is connected to one of those channels. The line of sight of the spectrometer in the present work is shown in Fig. 3 and is almost tangential to

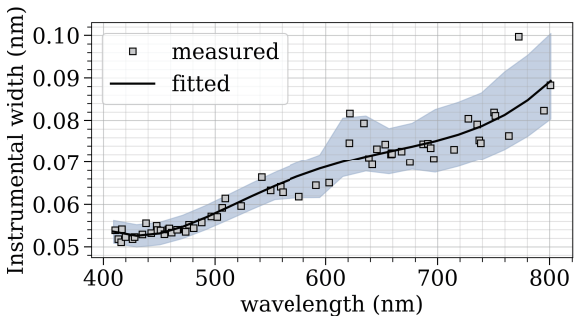

Fig. 4 Instrumental function of Echelle spectrometer ($1/e$ width σ_{inst}). The plot is fitted with a polynomial function. The standard deviation of the scattered data is shown as a colored shape.

the magnetic field lines. The spectrometer is looking at the divertor leg.

3. Results

The carbon impurity flow velocities and temperatures in hydrogen (H) and deuterium (D) discharges of the nineteenth cycle of LHD operation are investigated. The deuterium concentration $C(\text{D}) = N(\text{D})/(N(\text{H}) + N(\text{D}))$, where $N(\text{H, D})$ - number of hydrogen or deuterium atoms in plasma, in H was $C(\text{D}) = 0 - 0.25$ and in D $C(\text{D}) = 0.75 - 1.0$. Discharges with following parameters were selected. Magnetic axis $R_{\text{ax}} = 3.6\,\text{m}$, toroidal magnetic field $B_{\text{T}} = -2.75\,\text{T}$, three tangential neutral beams injected simultaneously with total power of 9 - 12 MW, line integrated electron density $n_{\text{e}} = (1 - 14) \times 10^{19}\,\text{m}^{-3}$, and the central electron temperature $T_{\text{e}} = 1.5 - 3.5\,\text{keV}$. Different ionization states of carbon impurity (C^{+}-C^{3+}) are studied here. The following emissions are used for analysis: C^{+}(CII, $1s^2 2s2p3s - 1s^2 2s2p3p$, 515.108 nm), C^{2+}(CIII, $1s^2 2s3s - 1s^2 2s3p$, 464.742 nm), and C^{3+}(CIV, $1s^2 5f - 1s^2 6g$, 465.751 nm $1s^2 5g - 1s^2 6h$, 465.846 nm). The carbon flow velocities and temperatures estimated from the Doppler shift and broadening are shown in Figs. 5 and 6, respectively.

In Fig. 5, negative velocities indicate the flow toward the divertor plates. It is found that for all selected discharges the flow is toward the divertor, and no changes in the direction are observed. Impurity flow velocities for D plasma are systematically slower, by the factor of 1.4 - 2, compared to H plasma. It is also found that the velocities of C^{+} and C^{2+} are faster than that of C^{3+}. That is, for C^{+} and C^{2+} they are in the range of 10 - 30 km/s, and they are in the range of 5 - 20 km/s for C^{3+} ions. In H discharges the impurity flow velocities increase, i.e., they become more negative with increasing plasma density, while in D discharges this dependency is weaker. At low densities in H discharges, there is a fast increase of velocities, especially in C^{2+} velocity.

In Fig. 6, the blue, orange, and green horizontal lines indicate ionization potentials for C^{+}, C^{2+}, and C^{3+} ions for

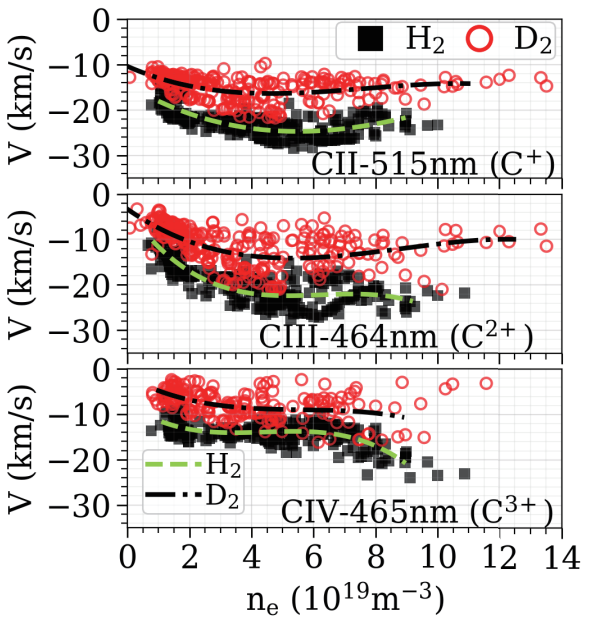

Fig. 5 Carbon impurity flow velocities. Black squares correspond to H discharges and red circles - to D. The data points with Gaussian fit errors smaller then 1 km/s are shown. Time averaged and smoothed data are plotted as green dashed (H) and black dash-dot (D) lines.

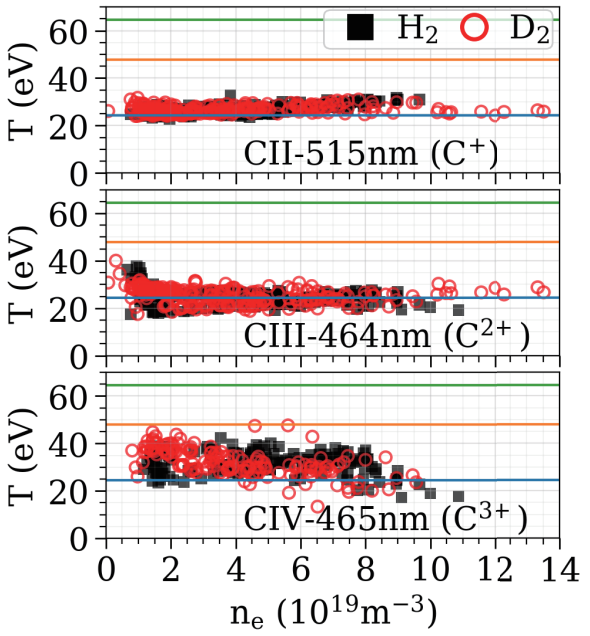

Fig. 6 Carbon impurity temperatures. Horizontal lines indicate ionization potential for C^{+},C^{2+} and C^{3+}. The data points with Gaussian fit errors smaller then 2.2 eV are shown.

reference, 23.38 eV, 47.89 eV, and 64.49 eV, respectively. In contrast to the velocity, temperatures of carbon ions in H and D plasmas are found to remain the same. The temperatures of C^{+} and C^{2+} are in the similar range and close to the ionization potential of C^{+}, while temperatures of C^{3+} extend to slightly higher values, but are significantly

lower than the ionization potential of C^{3+}. For C^{+} and C^{2+} the temperatures remain almost constant against density increase, except for the lowest density range, $< 2\times10^{19}$ m^{-3}, where rapid decrease is observed with density for C^{2+}. On the other hand, temperature of C^{3+} shows slight decrease with increasing density, while the scatter is large. In the modeling of the impurity transport it is commonly assumed that the impurity temperature is equal to the ion temperature, $T_Z = T_i$. The present experimental results of the different temperatures for different ionization states of carbon suggest the necessity to improve this modeling assumption.

4. Discussion

The isotope effects on the impurity velocity could be evaluated from the force balance equation. Considering the parallel momentum transport equation for impurity [9], the dominant forces are friction and ion thermal forces (temperature gradient force). In a steady state, balancing the tow forces reads,

$$V_Z = -V_i + C_i Z^2 \frac{\tau_s}{m_Z}\frac{\partial T_i}{\partial s}. \quad (2)$$

Here V_Z is the flow velocity of the impurity with charge Z, and V_i is the background ion (H or D) velocity in parallel direction which can be written as $V_i = M\,C_s$ with $C_s = \sqrt{\frac{T_i+T_e}{m_i}}$ and M being Mach number. T_i - ion temperature, m_Z - impurity ion mass, τ_s - slowing down time for impurity colliding with background plasma, and s - distance in parallel direction. C_i is a numerical factor of order 1. The sign of each term is such that the negative value is in the direction toward the divertor plates with $V_Z > 0$ and $\frac{\partial T_i}{\partial s} > 0$, the same as the definition in Fig. 5. With increasing density, the thermal force is overcome by friction force, which drives the impurity toward divertor plates through background plasma flow. This trend is observed in Fig. 5, where the flow velocity toward the divertor plates increases with increasing density for all charge states. The ion velocity has a mass dependence as $V_i \propto 1/\sqrt{m_i}$ and thus is smaller in D. The collision time is also inversely proportional to the square root of mass, $\tau_s \propto 1/\sqrt{m_i}$. The parallel temperature gradient can be expressed as

$$-\frac{\partial T_i}{\partial s} = \frac{q_{\|i}}{\kappa_i}, \quad (3)$$

where $q_{\|i}$ and κ_i are the parallel ion heat flux and parallel heat conductivity for ion. Since $\kappa_i \propto 1/\sqrt{m_i}$, given the same input power, $q_{\|i}$, $\frac{\partial T_i}{\partial s} \propto \sqrt{m_i}$. Therefore, the mass (isotope) effect in the second term of eq. 2 may compensate between τ_s and $\frac{\partial T_i}{\partial s_i}$. The remaining effect is a slowdown of the background plasma velocity, V_i, in deuterium due to the mass dependence. The ratio of $V_Z^{H,D}$ for H and D plasmas can be written as

$$\frac{V_Z^H}{V_Z^D} = \frac{-V_i^H + C_i Z^2 \frac{\tau_s^H q_{\|i}}{m_Z \kappa_i^H}}{-V_i^D + C_i Z^2 \frac{\tau_s^D q_{\|i}}{m_Z \kappa_i^D}}, \quad (4)$$

where the superscripts, H and D, denote the values for H and D plasmas. In a collisional limit, that is, in the high density range, $\tau_s \to 0$, thus, $V_i \gg C_i Z^2 \frac{\tau_s q_{\|i}}{m_Z \kappa_i}$ and $\frac{V_Z^H}{V_Z^D} \approx \frac{-V_i^H}{-V_i^D} \approx \sqrt{\frac{m_i^D}{m_i^H}} \sim 1.4$, which agrees with the trend observed in Fig. 5. In a collisionless limit, that is, low density range, $V_i \ll C_i Z^2 \frac{\tau_s q_{\|i}}{m_Z \kappa_i}$, and $\frac{V_Z^H}{V_Z^D} \approx \frac{\tau_s^H/\kappa_i^H}{\tau_s^D/\kappa_i^D} \sim 1$, because of the mass dependence of τ_s and κ_i as discussed above. This trend toward low density range may be observed in the flow of C^{+} and C^{2+}, although the tendency is weaker than the model prediction. In the case of C^{3+}, however, there is no such trend observed. One possible reason for this discrepancy is a kinetic effect that may prevail in the low collisional regime, which is not considered in the present formulation. The issue may be addressed in comparison with numerical simulation, which is left for future work.

The EMC3-EIRINE calculations in LHD, based on the above fluid model, predict impurity flow reversal in the low density range, i.e., flow toward upstream, which is caused by strong thermal force (temperature gradient force) acting on the impurity [3]. With increasing density, the thermal force is overcome by friction force, which drives the impurity toward divertor plates through the background plasma flow. In the present experiment, however, such flow reversal is not observed in both D and H discharges. This result indicates the need for improvement of the thermal force of fluid model, which tends to overestimate in low collisional regime [10, 11].

5. Summary

Echelle spectrometer with a wide wavelength range (409 - 801 nm) and with a high resolution (~ 0.05 nm) was installed and run for the latter half of the nineteenth experimental campaign in LHD. A processing tool for the spectroscopic image was developed to construct spectra from the raw 2D CCD images of the spectrometer. Flow velocities and temperatures of carbon impurities are evaluated for H and D plasmas in a wide density range.

It is found that, in both H and D plasmas, carbon flows toward the divertor plates in the whole density range without showing flow reversal as predicted by the edge impurity transport model. The results indicate the importance of the model improvement by taking into account a kinetic effect on the thermal force in the low density (low collisionality) range. For C^{+} and C^{2+} velocities are in the range of 10 - 30 km/s, and 5 - 20 km/s for C^{3+} ions.

A pronounced isotope effect on the impurity velocities is observed. In D discharges, the carbon flow of all ionized states is slower compared to H, by the factor of 1.4 - 2. Possible reason for this difference is discussed based on the parallel momentum balance of impurity, where the mass effect qualitatively explains the experimental results. It is also found that in H discharges velocities increase proportionally to the plasma density, while in D discharges this dependency is weaker.

It is also observed that the evaluated impurity temperatures are different, and show different density dependence between different ionization states. These data are informative and useful for further study of the impurity transport and model validation, which are left for future works.

Acknowledgments

This work has been financially supported by JSPS Grant No. 16H04622, and by the NIFS budget ULPP026 and KOAP031.

[1] E.J. Doyle, W.A. Houlberg, Y. Kamada *et al.*, Nucl. Fusion **47**, S18-127 (2007).
[2] P. Helander, S.L. Newton, A. Mollén *et al.*, Phys. Rev. Lett. **118**, 155002 (2017).
[3] M. Kobayashi, S. Morita, C.F. Dong *et al.*, Nucl. Fusion **53**, 033011 (2013).
[4] S. Dai, M. Kobayashi, G. Kawamura *et al.*, Nucl. Fusion **56**, 06605 (2016).
[5] T. Oishi, S. Morita *et al.*, Nucl. Fusion **58**, 016040 (2018).
[6] T. Nakano, H. Kubo, N. Asakura *et al.*, Nucl. Fusion **47**, 1458 (2007).
[7] M. Goto, J. Quant. Spectrosc. Radiat. Transf. **76**, 331 (2003).
[8] T. Shikama *et al.*, Plasma Fusion Res. **2**, S1045 (2007).
[9] P. Stangeby, *The plasma boundary of magnetic fusion devices* (IOP Publishing, Bristol and Philadelphia, 2000), p. 298.
[10] D. Reiser, D. Reiter and M.Z. Tokar, Nucl. Fusion **38**, 165, (1998).
[11] K. Shimizu, T. Takizuka, K. Ohya *et al.*, Nucl. Fusion **49**, 065028 (2009).